Modulation of synaptic strength at hippocampal synapses

A Thesis

submitted to

Indian Institute of Science Education and Research Pune in partial fulfillment of the requirements for the BS-MS Dual Degree Programme

by

Namit Dwivedi



Indian Institute of Science Education and Research Pune
Dr. Homi Bhabha Road,
Pashan, Pune 411008, INDIA.



State University of New York

Under the guidance of

Supervisor: Dr, Annalisa Scimemi,

State University of New york at Albany

From <u>May 2024</u> to <u>Mar 2025</u> INDIAN INSTITUTE OF SCIENCE EDUCATION AND RESEARCH PUNE

Certificate

This is to certify that this dissertation entitled "Modulation of synaptic strength at hippocampal synapses" towards the partial fulfilment of the BS-MS dual degree program at the Indian Institute of Science Education and Research, Pune represents work carried out by Namit Dwivedi at State University of New York at Albany under the supervision of Dr. Annalisa Scimemi, Associate Professor, Department of Biology, during the academic year 2024-2025.

Annalisa Scimemi

26/03/2025

Supervisor: Dr. Annalisa Scimemi

Expert: Dr. Suhita Nadkarni

"This thesis is dedicated to anyone and everyone who has ever doubted themselves or felt out of place."

Declaration

I hereby declare that the matter embodied in the report entitled "Modulation of synaptic strength at hippocampal synapses" are the results of the work carried out by me at the Department of Biology, State University of New York at Albany, under the supervision of Dr. Annalisa Scimemi and the same has not been submitted elsewhere for any other degree

Namit Burivedi

Namit Dwivedi 20201108 March 16, 2025

Table of Contents

| Declaration | 5 |
|---|----|
| Table of Contents | 6 |
| Abstract | 7 |
| Acknowledgments | 8 |
| Author contributions | 9 |
| Chapter 1- Introduction | 10 |
| Glutamatergic transmission in the neocortex | 10 |
| General classification of glutamate receptors | 10 |
| GABAergic Transmission | 11 |
| General classification of GABA receptors | 11 |
| Subcellular distribution of GABA _A receptors | 12 |
| What preserves spatially confined synaptic transmission? | 12 |
| Changes in glutamate/GABA transmission in Alzheimer's disease | 13 |
| Neuronal and astrocytic contributions to Alzheimer's disease | 14 |
| Hypothesis | 14 |
| Chapter 2 - Materials and Methods | 15 |
| 2.1 NEURON model of CA1-PCs in voltage-clamp mode | 15 |
| The NEURON simulation environment | 15 |
| NRN-EZ | 15 |
| lon channel distribution | 16 |
| Space clamp errors | 16 |
| 2.2 NEURON model of CA1-PCs in current-clamp mode | 16 |
| lon channels | |
| Distribution of synaptic weights | |
| Chapter 3 - Results | |
| Modeling voltage clamp errors in CA1-PC | 19 |
| Miniature IPSC recordings | |
| Restricting the spatial distribution of the inhibitory inputs | 21 |
| Setting the release probability of inhibitory inputs | 22 |
| Effect of glutamate spillover on proximal and distal inhibition | 23 |
| Determining the synaptic weight of the excitatory synapses | 26 |
| Effect of Aβ ₄₂ on integration of excitatory and inhibitory inputs | 27 |
| Chapter 4 - Discussion | 29 |
| References | 30 |

Abstract

Glutamate is the major excitatory neurotransmitter in the mammalian brain. Once released into the synaptic cleft, glutamate is cleared within less than a millisecond through passive diffusion and active uptake. The efficiency of these processes depends on the morphology of the synapse and extracellular space and the spatial distribution of glutamate transporters, abundantly expressed in astrocytes. Only a perimeter of 50% of hippocampal excitatory synapses is by astrocytic membranes, leaving ample room for glutamate to act at non-synaptic sites. Glutamate spillover can lead to the activation of receptors expressed on neighboring GABAergic interneurons, a process that can be exacerbated by blocking glutamate transporters. Our slice physiology experiments show that glutamate spillover leads to heterosynaptic activation of presynaptic metabotropic glutamate receptors expressed at neighboring GABAergic terminals. Here, we show that this form of presynaptic modulation occurs at different types of GABAergic neurons targeting CA1 pyramidal cells. In addition, we provide an example of changes in synaptic strength that happen through various forms of modulation in CA1 pyramidal cells in the presence of $A\beta_{42}$, a peptide that accumulates in the brain of patients affected by Alzheimer's disease. By using a compartmental model of these cells, we explore the implications that concurrent changes in synaptic strength have on the firing output of the hippocampus. These findings shed light on the implications that small changes in synaptic strength have to regulate the activity of neuronal circuits implicated with learning, memory, and spatial navigation.

Acknowledgments

I would like to express my sincere gratitude to my supervisor, Dr. Annalisa Scimemi, for her unwavering support, insightful guidance, and patience throughout this project. Her approachability and willingness to engage in detailed discussions whenever I felt stuck were invaluable to my growth as a researcher.

I am also deeply thankful to Maurice Petroccione for generously taking the time to explain his work step by step. His detailed insights into the experimental protocols, which I was initially unfamiliar with as a computational researcher, helped me better understand the broader biological context and the nuances that shaped the modeling process.

My sincere thanks go to Ethan Caizzara, Anthony Manning, Leonardo Frasson dos Reis, and Dr. Phillip Albrecht for their thoughtful feedback during lab meetings and for creating a collaborative, friendly, and motivating lab environment.

I am also grateful to my expert mentor, Dr. Suhita Nadkarni, for her valuable feedback during the mid-year report and for her continuous encouragement and support — even before I arrived in the US.

Finally, I would like to thank IISER Pune for enabling me to pursue a 10-month thesis project under an external supervisor, which greatly enriched my academic and research experience.

Author contributions

| Contribution | Contributor |
|------------------------------|-------------------------------------|
| Conceptualization ideas | Dr. Annalisa Scimemi, Namit Dwivedi |
| Methodology | Namit Dwivedi |
| Software | Namit Dwivedi |
| Validation | Dr. Annalisa Scimemi |
| Formal analysis | Namit Dwivedi |
| Investigation | Dr. Annalisa Scimemi, Namit Dwivedi |
| Resources | Dr. Annalisa Scimemi |
| Data curation | Dr. Annalisa Scimemi, Namit Dwivedi |
| Writing - original draft | Namit Dwivedi |
| Writing - review and editing | Dr. Annalisa Scimemi, Namit Dwivedi |
| Visualization | Dr. Annalisa Scimemi, Namit Dwivedi |
| Supervision | Dr. Annalisa Scimemi |
| Project administration | Dr. Annalisa Scimemi |
| Funding acquisition | Dr. Annalisa Scimemi |

Chapter 1- Introduction

Glutamatergic transmission in the neocortex

Glutamate is the most abundant excitatory neurotransmitter in the mammalian brain. Most vital functions like cognition, memory, and learning are mediated by glutamate (Fonnum 1984). Disrupting the time course of the glutamate concentration profile in or outside the synaptic cleft can have profound implications for shaping the brain's ongoing activity and may also contribute to neurodegenerative disease. The mammalian brain contains a large amount of glutamate (about 5-15 mmol/Kg wet weight, although this can vary across brain regions (Danbolt 2001). However, its concentration in the cerebrospinal fluid is maintained at ~25 nM (Chiu and Jahr 2017; Herman and Jahr 2007). This is thought to be achieved through the activity of a large population of glutamate transporters, abundantly expressed in astrocytes (Lehre and Danbolt 1998). Glutamatergic transmission is mediated by glutamate receptors, which can be expressed pre- and post-synaptically at excitatory glutamatergic synapses and pre-synaptically at inhibitory synapses release the neurotransmitter y-aminobutyric acid (GABA). There are different types of glutamate receptors with different binding affinities and kinetics. Therefore, changes in the time course of synaptically released glutamate in the extracellular space can exert different functional effects depending on the spatial distribution and molecular identity of the glutamate receptors that can be activated. n. Because glutamate can also mediate excitotoxicity, it is crucial to maintain extracellular glutamate concentration within a critical concentration range, which ensures synaptic transmission without triggering cytotoxicity.

General classification of glutamate receptors

There are two main classes of glutamate receptors: (i) ionotropic and (ii) metabotropic. receptors be The ionotropic can further subdivided into (i) α -amino-3-hydroxy-5-methyl-4 isoxazolepropionic (AMPA) receptors: acid (ii) N-Methyl-D-aspartate (NMDA) receptors; (iii) kainate receptors.

All ionotropic glutamate receptors are mixed cationic channels, meaning that they are permeable to Na⁺, K⁺, and, in some cases, Ca²⁺. AMPA and NMDA receptors are more abundantly expressed than kainate receptors and have received substantial attention for scientific investigations by the international neuroscience community. Therefore, this work will mostly focus on AMPA and NMDA receptors. Studies in expression systems have shown that ionotropic glutamate receptors form tetrameric assemblies (dimers of dimers), and their functional properties depend on their subunit composition (Sommer et al. 1991). AMPA receptors are composed of GluA1–GluA4 subunits, are permeable to Na⁺ and K⁺, and are responsible for rapid depolarisation of the postsynaptic membrane potential. Some AMPA receptors, lacking the GluA2 subunit, are also permeable to Ca²⁺. By contrast, NMDA receptors are composed of GluN1, GluN2A-D, and GluN3 subunits and are permeable to Na⁺, K⁺, and Ca²⁺ ions. NMDA receptor opening requires the finding of both glutamate and glycine/D-serine as co-agonists. They are also

voltage-dependent due to a Mg²⁺ block (Mayer, Westbrook, and Vyklický 1988; Nowak et al. 1984). AMPA receptors have fast activation and desensitization, mediating the most rapid excitatory transmission. NMDA receptors have slower activation and deactivation and play a critical role in synaptic plasticity and learning.

Metabotropic glutamate receptors (mGluRs) are G-protein-coupled receptors (Masu et al. 1991). These receptors can be subdivided into three structurally and functionally homologous subgroups: mluRI (mGluR1 and mGluR5), mGluRII (mGluR2 and mGluR3), and mGluRIII (mGluR4, mGluR6, mGluR8, mGluR6 expressed in the retina). mGluRs are expressed in a cell type- and subcellular domain-specific manner by hippocampal neurons (Somogyi et al. 2003); (Shigemoto et al. 1996). mGluRI receptors are mostly expressed post-synaptically and in astrocytes. mGluRII and mGluRIII are mostly expressed presynaptically mGluRII and mGluRIII activation suppresses neurotransmitter release mirroring that of other presynaptic receptors (Vizi, 1979). Presynaptic mGluRIII inhibit the release of both glutamate and GABA in the hippocampus as well as in other brain regions, indicating they exert a crucial modulatory function in synaptic activity ((Gereau and Conn 1995); (Desai et al. 1994); (Baskys and Malenka 1991); (Scanziani, Gähwiler, and Charpak 1998); Morishita & Alger, 2000; (Morishita, Kirov, and Alger 1998); (Poncer, Shinozaki, and Miles 1995); (Semyanov and Kullmann 2000); Schrader & Tasker, 1997; (Salt and Eaton 1995). This modulatory effect limits neuronal excitation, which is crucial to ensure normal brain functioning and prevent excitotoxicity.

GABAergic Transmission

GABA is the primary inhibitory neurotransmitter in the mammalian central nervous system. It plays a crucial role in reducing neuronal excitability. Much like glutamate, GABA is critical for various neural functions, including mood regulation, pain perception, and reducing neuronal excitability (Bowery, 1989; Mody et al., 1994). The balance between glutamatergic and GABAergic transmission is essential for brain function, and dysregulation in GABA signaling is implicated in numerous neurological disorders, such as epilepsy, anxiety disorders, and schizophrenia (Olsen & Avoli, 1997; Möhler, 2007). GABA concentration is regulated both within synaptic vesicles and in the extracellular space to modulate receptor activation (Sivilotti & Nistri, 1991; Kaila & Voipio, 1987).

General classification of GABA receptors

GABA binds to GABA_A, GABA_B, and GABA_c receptors (Bormann 2000). Both GABA_A and GABA_P receptors are ligand-gated chloride channels (thus permeable to chloride), whereas GABA_B are metabotropic receptors. The GABA_A receptor consists of five subunits (i.e., they are pentamers), and the transmembrane domains of the subunits form a central ring of positive charges surrounding the permeability pore for Cl⁻ ions. The reversal potential for Cl⁻ is usually far more negative as compared to the threshold for firing an action potential, but very close to the resting membrane potential of

neurons. Therefore, depending on the driving force, GABA_A receptor opening can cause voltage inhibition (if $E_{\text{Cl}} < V_m$) or shunting inhibition (is $E_{\text{Cl}} \sim V_m$) (Farrant and Nusser 2005). Shunting inhibition is due to reduced membrane resistance due to GABA_A receptor opening, not associated with a change in membrane potential. The most common subunit composition of GABA_A receptors in the brain is: 2α , 2β , and 1γ (e.g., $\alpha_1\beta_2\gamma_2$ is the most abundant). The presence of the γ -subunit allows benzodiazepine binding (e.g., diazepam, lorazepam). The presence of the δ -subunit is mostly detected in extrasynaptic regions and allows these GABA_A receptors to mediate tonic inhibition (e.g., $\alpha_4\beta\delta$ or $\alpha_6\beta\delta$).

 GABA_B receptors are metabotropic, G protein-coupled receptors that mediate slower and more prolonged inhibitory signals by regulating the opening of K^+ and Ca^{2+} channels (Bettler, Kaupmann, and Bowery 1998; Bettler et al. 2004). These receptors modulate synaptic plasticity, neuron excitability, and neurotransmitter release. The structure of the GABA_B receptor is very similar to that of metabotropic receptors, although these assemble as the heterodimers of two subunits called B1 and B2.

GABA_c receptors are a subclass of GABA receptors primarily composed of ρ subunits ($\rho1-\rho3$). Unlike GABA_A receptors, GABA_c receptors are insensitive to benzodiazepines and barbiturates and have slower, more prolonged inhibitory effects. They are predominantly found in the retina, where they regulate visual processing, but have also been identified in other brain regions. GABA_c receptors function as Cl⁻-permeable ion channels, similar to GABA_A receptors, but exhibit distinct pharmacological and kinetic properties that allow them to mediate sustained inhibition. (Enz and Cutting 1999).

Subcellular distribution of $GABA_A$ receptors

GABA_A receptors can have not only a very diverse subunit composition, which shapes their biophysical properties, but they are also heterogeneously distributed across neuronal cell membranes (depending on their subunit composition). GABA_A receptors with different subunit compositions are differentially distributed between the synaptic and extrasynaptic regions. Electron microscopy studies using immunogold labeling have shown that many GABA_A receptors (containing the γ -subunit) are densely packed at postsynaptic sites opposite to GABAergic terminals, thereby facilitating rapid synaptic inhibition (Nusser et al. 1996). Other GABA_A receptors (containing the α_5 - or δ -subunit) are present in extrasynaptic regions, and their activation contributes to mediate tonic inhibition (Farrant and Nusser 2005); (Brickley and Mody 2012). , thereby tailoring inhibitory control to the functional requirements of specific neuronal circuits.

What preserves spatially confined synaptic transmission?

The textbook model of synaptic transmission posits that neurotransmitters released at the synapse act locally on postsynaptic receptors and are cleared from the synaptic cleft within a millisecond (Clements et al. 1992). Most glutamate transporters are located

outside the synaptic cleft, in neighboring astrocytic processes. These molecules constitute an efficient uptake system that limits neurotransmitter diffusion out of the synaptic cleft, preserving the spatial specificity of point-to-point synaptic transmission (Hille 1992). Therefore, the 3D organization of the tripartite synapse promotes rapid glutamate clearance. Under certain physiological and pathological circumstances, for example, when glutamate transporters are close to saturation or when their expression is reduced, glutamate can diffuse out of the synaptic cleft. This phenomenon is commonly referred to as glutamate spillover. This can lead to activation of neighboring presynaptic mGluRs. Since only 50% of the perimeter of these synapses is contacted by astrocytic membranes, this leaves ample room for glutamate to act at non-synaptic sites (Herde et al. 2020; Scanziani et al. 1997; Ventura and Harris 1999). The phenomenon by which glutamate diffuses to neighboring synapses is commonly referred to as glutamate spillover (Semyanov and Kullmann 2000; Vogt and Nicoll 1999). Glutamate spillover can lead to the activation of receptors expressed on neighboring GABAergic interneurons (INs). This form of modulation of synaptic transmission is called heterosynaptic, meaning that release from one synapse affects neighboring synapses releasing different neurotransmitters. mGluRs are expressed preand post-synaptically at excitatory and inhibitory hippocampal synapses (Vogt and Nicoll 1999). For example, in the hippocampus, glutamate spillover can lead to the activation of mGluRs expressed in axonal boutons of GABAergic neurons, reducing GABA release (Bloss et al. 2016).

Changes in glutamate/GABA transmission in Alzheimer's disease

Alzheimer's disease (AD) is a chronic, progressive neurodegenerative disorder that represents the most prevalent form of dementia in the elderly population, accounting for approximately 60–80% of dementia cases (Alzheimer's Association 2014). It is characterized clinically by a gradual decline in cognitive functions such as language, memory, reasoning, and executive function, ultimately leading to a loss of independence and death. However, the pathological changes in the brain often begin years or even decades before the onset of noticeable symptoms, making early detection and intervention almost impossible.

At the molecular and cellular levels, the two classical hallmarks of AD pathology are the extracellular deposition of amyloid-beta (A β) plaques and the intracellular accumulation of hyperphosphorylated tau protein into neurofibrillary tangles. A β peptides are produced by the sequential cleavage of the amyloid precursor protein (also known as APP) by β - and γ -secretases. Recent reports from autosomal dominant forms of AD suggest that A β accumulation may be evident 20 years before the stage of dementia and that there is already substantial neuronal loss by the stage of mild cognitive impairment (Sperling, Mormino, and Johnson 2014). Among the isoforms generated, A β_{42} is particularly prone to aggregation and neurotoxicity. These peptides oligomerize and eventually form insoluble plaques that disrupt cell-to-cell communication, promote oxidative stress, and trigger inflammatory responses in the brain (Selkoe & Hardy, 2016).

Neuronal and astrocytic contributions to Alzheimer's disease

A large body of work has shown that neuronal death and astrogliosis can be detected postmortem in the AD brain. This suggests that neurons, astrocytes, and synapses are key targets of this disease. Recent transcriptome work, however, shows that not all neuronal and non-neuronal cells are affected at the same time during the progression of this disease (Gabitto et al. 2024). Specifically, somatostatin (SST) INs show changes in gene expression and morphology early on, during mild cognitive impairment, followed by changes in the anatomical and functional properties of glutamatergic neurons and then parvalbumin (PV) INs and microglial and astrocytic cells. These findings are important as they highlight cell-specific changes that occur during disease progression. This suggests that the development of novel strategies for early diagnosis and therapeutic intervention may change depending on the stage of AD.

Hypothesis

In CA1 pyramidal cells (CA1-PCs), proximal inhibition is largely provided by PV-INs, whereas distal inhibition is provided by SST-INs. PV-INs form synapses on the soma and apical dendrites (<50 µm from the soma). SST-INs form synapses on the apical dendrite (>200 µm away from the soma)(Bloss et al. 2016; Danbolt 2001). Dihydorokainic acid (DHK) is an inhibitor of the main glutamate transporter in the adult brain, GLT-1 (Danbolt 2001; Scanziani et al. 1997). By inhibiting glutamate uptake via GLT-1, DHK promotes glutamate spillover from the synaptic cleft. In slice physiology experiments, glutamate spillover leads to heterosynaptic activation of presynaptic mGluRIIIs expressed at GABAergic terminals onto CA1-PCs and onto other INs. mGluRIIIs are coupled to Gi/o proteins, which inhibit presynaptic Ca²⁺ channels, activate K⁺ channels, and suppress adenylyl cyclase (AC) activity. This cascade reduces cAMP production and downstream PKA activation, thereby suppressing vesicle fusion and GABA release (Scanziani et al. 1997; Semyanov and Kullmann 2000). Reduced PKA activity leads to dephosphorylation of synapsins, decreasing their ability to maintain vesicles at release sites, and thereby shrinking the RRP without affecting release probability (P) or quantal size (q). This mechanism was confirmed in our lab by showing that the mGluRIII-mediated reduction in IPSC amplitude was blocked by PKA inhibitors and reversed by inhibiting the phosphatase calcineurin, which normally promotes synapsin dephosphorylation. This eventually leads to a reduction of inhibition onto CA1-PCs. The experiments from the lab indicate that the effect of DHK is similar when GABA release is evoked by optogenetic stimulation of PV- or SST-INs.

Given that these cells target different subcellular compartments, GABAergic inhibition via SST-INs is subject to larger electrotonic attenuation than the one mediated by PV-INs. Here, we ask whether this can confound the interpretation of the effects of glutamate spillover on mGluRIIIs in the axon of PV-and SST-INs.

Our preliminary slice physiology data (collected by the other lab members) show that $A\beta_{42}$, a peptide that accumulates in the brain of AD patients, might disrupt in different ways PV- and SST-inhibition onto CA1-PCs. Data from the lab shows that there are 3.3 times more PV inputs in the hippocampus of mice injected with an adeno-associated virus (AAV) encoding, $A\beta_{42}$. These mice are used 3-8 weeks post-transfection in the hippocampal area CA1. Though the number of SST inputs didn't change in $A\beta_{42}$, this made us question how these effects ultimately shape the input-output relationship and the firing output of CA1-PCs. By understanding these effects, we aim to define the functional effects of $A\beta_{42}$ for the pathogenesis of AD.

Chapter 2 - Materials and Methods

Our first goal was to closely replicate the experimental observations concerning the influence of glutamate spillover on both the distal and proximal regions of the CA1-PC. To achieve this, we incorporated a space clamp mechanism into our model. This addition was designed to mimic the experimental conditions, allowing for voltage escape and attenuation of current akin to those observed in laboratory settings. Subsequently, we adjusted the synaptic weights for the inhibitory inputs to ensure our simulation outputs aligned with the experimental data. All the simulations were run on a Dell PC (Microsoft Windows 10 Enterprise; 12th Gen Intel(R) Core i7-12700; 16 GB RAM, 1 TB HD) using the software NRN-EZ v1.1.6 (Cobb, Petroccione, and Scimemi 2023) and NEURON v7.6 (Hines and Carnevale 1997). We used Visual Studio Code (VS Code) as a user interface for both software.

2.1 NEURON model of CA1-PCs in voltage-clamp mode

We built a compartmental model of CA1-PCs using the 3D morphology of a biocytin-filled CA1-PC generated previously by our lab (https://www.neuromorpho.org). All files pertaining to the NEURON simulations were uploaded to the ModelDB database (https://senselab.med.yale.edu/modeldb/, ModelDB acc.n. 000). The first NEURON model was created to reproduce the results of the voltage-clamp experiments described in **Fig. 1** was run on Microsoft Visual Studio Code as an IDE.

The NEURON simulation environment

The nervous system processes information through the propagation and interaction of signals. These signals can be either chemical or electrical which are distributed across space and time. To investigate the underlying mechanisms that govern these signals, biologically realistic modeling is essential. This helps in a better understanding of how nervous system function emerges from the operation of these mechanisms. The NEURON simulation environment offers a powerful and flexible platform for constructing and analyzing models of individual neurons and small neuronal networks. (Hines and Carnevale 1997). In our models, we used NEURON by integrating it with Python and running spike simulations into our 3D morphology of CA1-PC.

NRN-EZ

NRN-EZ software application facilitates biophysical modeling within the NEURON simulation environment (Cobb, Petroccione, and Scimemi 2023). In our experiments, NRN-EZ was used to position synapses along the neuronal dendrites accurately. These synapses can be configured as excitatory or inhibitory depending on the user-defined parameters. In our model, we focused on investigating the inhibitory postsynaptic potentials (IPSCs) generated by GABAergic inputs. Specifically, the model included PV inputs localized within the first 50 μ m of the dendrite and SST inputs, randomly

distributed from 200 μ m to the distal end of the apical dendritic tree, approximately 550 μ m. Setting the parameters of these synapses in NRN-EZ, such as the reversal potential, rise & decay time, number of inputs, and their distance from the soma, NRN-EZ generates a run_1 folder. This folder, along with the morphology of the cell, contains the synaptic parameters associated with this excitatory/inhibitory synapse. One of these is a syn_loc.dat file that contains the compartments where the synapse is desired based on the entered parameters. This file, when incorporated in the Python code, can simplify the process of creating these synapses in the NEURON simulation environment.

Ion channel distribution

Voltage clamp is a recording mode used in patch-clamp electrophysiology to gain information about the currents generated by ion channel opening. In voltage clamp whole-cell patch-clamp recordings, experimenters use cesium-based internal solutions to block leak K⁺ channels to achieve a better clamp of the cell membrane potential. Given the extremely ramified morphology of CA1-PCs, not all leak channels may be completely blocked, especially in distal dendrites. This effect, generally referred to as space clamp, is discussed in more detail below. Briefly, to replicate our experimental observations and include the effects of space clamp artifacts in our computational model, we introduced distance-dependent passive potassium channels. These channels were essential for reproducing the phenomenon of voltage escape observed in experimental patch clamp experiments.

Space clamp errors

Because cell bodies are the largest compartments of neurons, most voltage clamp whole-cell patch-clamp recordings are obtained from neuronal somas. Given the close proximity between the soma and the axon initial segment - the site of origin of action potentials - somatic recordings are also useful to determine how synaptic inputs are converted into different types of outputs. When applied to spherical cells, a voltage clamp allows every point on the plasma membrane to rest at the same holding potential through a voltage clamp amplifier. However, in nonspherical cells like neurons, the voltage command imposed at the soma drops along dendrites due to the axial resistance of these compartments, where synaptic inputs arrive. As a result, the effective membrane potential of distal dendrites varies from the one imposed through the patch pipette when performing somatic voltage-clamp recordings. There are two key components that make a space clamp inadequate. First is the attenuation along the long neuronal cables and other is the reduction in driving force at the synapse caused by local hyperpolarization or depolarization (voltage escape) (Häusser and Roth 1997).

2.2 NEURON model of CA1-PCs in current-clamp mode

Building on our previous voltage-clamp model, we replaced the voltage clamp with a

current clamp to observe the dynamic voltage changes in our $A\beta_{42}$ -accumulated mouse models. NEURON utilizes MOD files, written in the NMODL programming language, to introduce custom mechanisms and ion channel dynamics. Since the initial model used a voltage-clamp configuration with all ion channels blocked, we incorporated relevant ion channels into the current-clamp model. To achieve this, we integrated MOD files from one of the previous CA1-PC models in our lab (McCauley et al. 2020) and compiled them with the model code. These MOD files contained parameters such as ion channel density and conductance values, which, once compiled, could be modified from the code. The code was written for both WT and $A\beta_{42}$ mouse models.

Ion channels

The current clamp model included the active conductances of the following channels: A-type potassium channels (KA), delayed rectifier potassium channels (KDR), voltage-gated sodium channels (Nav) Calcium-activated Potassium channels (Cagk), L-type Calcium channels (CaL), N-type Calcium channels (Can), and t-type Calcium channels (Cat). The conductances and distribution of the channels were described in the previously carried CA1-PC current clamp studies (Bloss et al. 2016; Migliore et al. 2018). The conductance of the Nav channels was close in range to as used by (Bloss et al. 2016; Migliore et al. 2018) in the field with gNa= 0.035 S/cm² (except for soma gNa=0.1 S/cm²). The conductances of all types of calcium channels were adapted from previous work by Migliore.

Table 1. Model Parameters

| V _{rest} | -65 mV |
|------------------------------|-------------------------|
| Temperature | 35°C |
| g_na (at axon and dendrites) | 0.035 S/cm ² |
| g_na (at Soma) | 0.1 S/cm ² |
| R _m | 40,000 |
| g_kdr | 0.04 S/cm ² |
| g_hd | 0.03 S/cm ² |
| R _a (except axon) | 150 ohm*cm |
| R _{aAxn} | 50 ohm*cm |
| V_{leak} | -65 mV |
| E _k | -90 mV |
| Ena | 60 mV |

| IClamp _{amp} | 0 A |
|-----------------------|-----|
| amp | 7 |

The A-type distance-dependent potassium channels were classified as proximal A-type potassium channels (Kap) and distal A-type potassium channels. These were distributed similarly to those adopted in previous computational studies. Channels that were more than 50 μ m away from the soma were considered distal, whereas those within 50 μ m from the soma. The conductance of the h-type distance-dependent channels was given by the equation:

$$ghd = 0.0005 * (1 + 3 * distance / 100)$$

If the distance for the section was less than 100 µm, then:

$$V_{halflife}$$
 = -81 mV

Whereas if it was more than 100 µm, then:

$$V_{halflife} = -73 \text{ mV}$$

Distribution of synaptic weights

All excitatory and inhibitory synapses were a two-state kinetic scheme synapse described by a rise time (τ_1) and decay time (τ_2) defined as the Exp2Syn in NEURON. This mechanism is particularly useful for simulating synaptic inputs where the conductance changes in response to a presynaptic spike follow an exponential rise and an exponential decay. Mathematically, the synaptic current is modeled using an alpha function-like conductance profile, particularly when τ_1 and τ_2 are approximately equal. The equation governing this conductance is given by:

$$g = weight * factor * (e)^{-(t/\tau_2)} - (e)^{-(t/\tau_1)}$$

where *g* represents the conductance, and t denotes time. The 'weight' parameter is derived from the weight field of a NetCon object in NEURON, which is used to scale the synaptic strength, and the 'factor' is calculated such that the normalized peak conductance reaches 1.

Chapter 3 - Results

Previous studies suggested that mGluRIII selectively inhibits glutamate and GABA release at synapses onto CA1-INs but not CA1-PCs. These conclusions, however, were based on experiments in which the concentration of extracellular calcium ([Ca²+]₀) was more than two times higher than that present in the cerebrospinal fluid. This led us to question whether the non-physiological levels of [Ca²+]₀ used in these experiments could have masked a function of mGluRIII in the brain.

To test the effect of spillover-mediated mGluRIII activation on IPSCs, patch clamp experiments were conducted in the lab to observe the evoked IPSCs in CA1-PCs. The ionotropic glutamate receptor blockers NBQX (10 µM) and APV (50 µM) were added to the bath of the CA1-PCs. DHK (100 µM) was added to inhibit glutamate uptake by GLT-1 (a major glutamate transporter expressed in astrocytes) to promote glutamate spillover and mGluRIII activation. When these experiments were performed at [Ca²⁺]₀=2.5 mM, DHK did not change the IPSC amplitude or kinetics (amp: 93±14%, p=0.66; t_{50} : 105±10%, p=0.62; rise: 96±10%, p=0.73, n=10). However, when [Ca²⁺]_o was adjusted to physiological levels (1.2 mM), DHK significantly reduced the IPSC amplitude without affecting its kinetics (amp: $69\pm6\%$, ***p=8.8e-5; t_{50} : $93\pm4\%$, p=0.13; rise: 100±7%, p=0.96, n=15). To verify that this effect was due to mGluRIII activation, we repeated these experiments in the continuous presence of the mGluRIII antagonist, MSOP (100 µM). MSOP blocked the effect of DHK on the IPSC amplitude and kinetics (amp: $98\pm9\%$, p=0.82; t_{50} : $91\pm5\%$, p=0.15; rise: $103\pm16\%$, p=0.88, n=7). Together, these results suggest that mGluRIII activation via spillover reduces GABAergic inhibition onto CA1-PCs, but only at physiological concentrations of [Ca²⁺]₀.

In CA1-PCs, proximal inhibition is provided by PV-INs, whereas distal inhibition is provided by SST-INs. Given that these cells target different subcellular compartments, GABAergic inhibition via SST-INs is subject to larger electrotonic attenuation than the one mediated by PV-INs. So we then asked whether mGluRIII equally contributes to inhibition arriving at both the proximal and distal dendrites of CA1-PCs.

Modeling voltage clamp errors in CA1-PC

As established earlier, the distal inputs are subjected to larger attenuation compared to the inputs that target the proximal subcellular compartments. This attenuation is a function of distance and varies with it exponentially. We needed to incorporate space clamp errors in our compartmental model to replicate the patch-clamp recordings taken at the soma experimentally. This will attenuate the currents generated at the different subcellular compartments in the model at the same rate at which the oIPSCs are attenuated in the experimental reading. We established the spatial distribution of inhibitory GABAergic synapses on the apical dendritic tree of CA1-PC using NRN-EZ. The 3D morphology of the CA1-PC was imported into NRN-EZ (v1.1.6), where we stochastically allocated 100 GABAergic synaptic inputs along the apical dendritic tree, spanning approximately 500 µm radially. The input locations were randomly assigned

within a radial distance of 250 \pm 250 μ m to account for dendritic signals from different subcellular compartments. The ratio between the current recorded locally at the dendrite and the current recorded at the soma was calculated by each individual input. To alter these readings to match with the experimental data, we introduced passive potassium channels along the dendrites to reproduce the space clamp errors. The conductance of these channels became larger with the increasing distance from the soma. We scaled *gpas* such that g_{pas} =10-5e(d/100) S/cm², where d is the distance of each compartment from the soma. This formalism allowed us to match the attenuation ratio of our model to that reported by (Williams and Mitchell 2008) (**Fig. 1a, b, d**) using dendritic patch clamp recordings from CA1-PC and the theoretical estimates of (Li et al. 2019) (**Fig. 1c**) The local rise and decay time were matched to the referenced studies to compare the results more accurately. The individual current traces from varied distances (100, 300, and 500 μ m away from the soma as shown in the **Fig.1b-d**) show depreciating current recorded at the soma in comparison to the inhibitory postsynaptic current recorded locally at the dendrite.

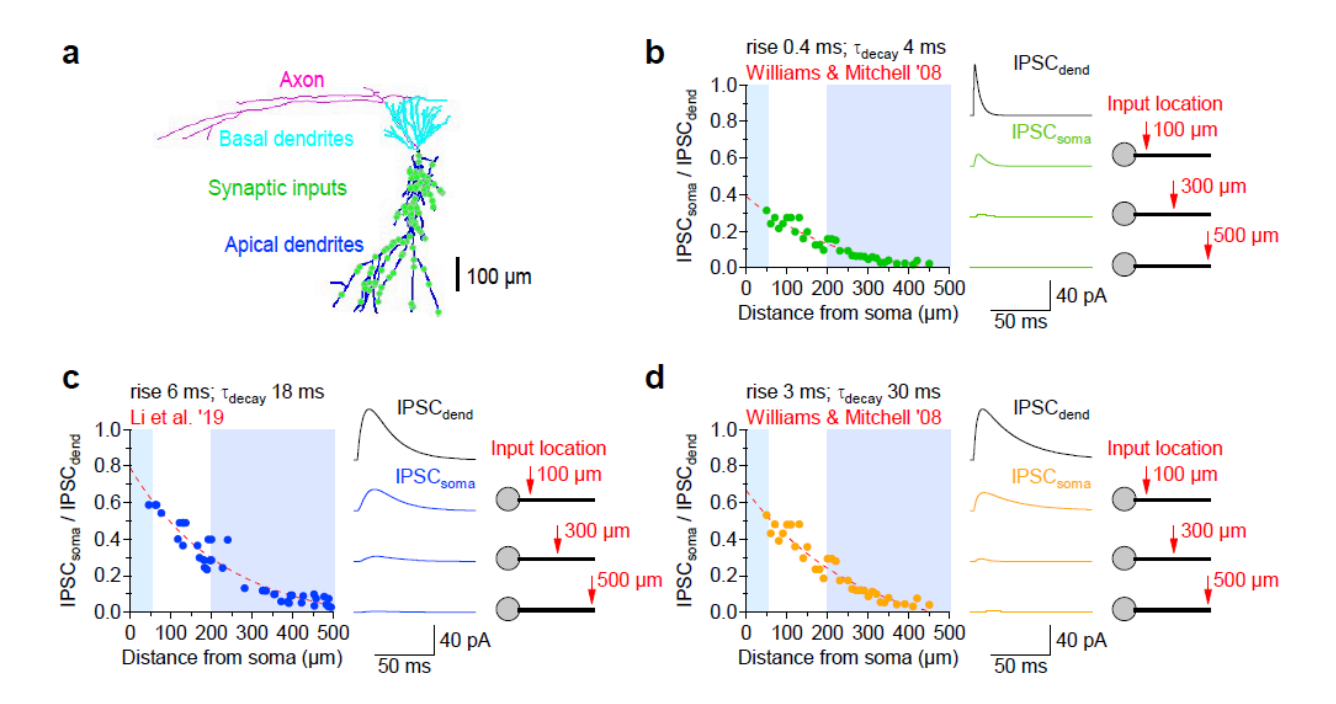


Figure 1. Parameter optimization for voltage-clamp model of CA1-PCs. (a) Morphology of the CA1-PC used to run the NEURON compartmental model, with 100 inputs distributed randomly throughout the soma and apical dendrites (*green dots*). **(b-d)** Quantification of the distance-dependent loss of current at the soma for IPSCs generated at different dendritic locations. Introducing a leak conductance allows reproducing the somatic voltage clamp loss reported in the literature using dendritic recordings ^{64,109}. The traces represent the inhibitory currents injected in dendrites located 100, 300, and 500 μm away from the soma (*black*) and their corresponding somatic recordings (*green, blue, orange*).

Constraining synaptic weight for miniature IPSC recordings

In NEURON, the synaptic strength is modulated using the weight[0] attribute of the NetCon object. For Exp2Syn synapses, this weight value directly corresponds to the peak synaptic conductance (in µS). For our model, we used a conductance-based mechanism, and the value of weight was adjusted to replicate the amplitude and kinetics of experimentally observed mIPSCs in CA1 pyramidal neurons. Once the relationship between gpas and d was set, we performed separate simulations to constrain the synaptic weight of each inhibitory input. Previous electrophysiological studies on layer 5 pyramidal neurons have demonstrated that significant distortions in synaptic conductance values occur at distances >200 µm from the soma (Williams and Mitchell 2008). So, the miniature IPSCs (mIPSCs) were modeled under the assumption that in many neocortical neurons, voltage escape prevents recording the activity of synaptic inputs located >200 mm from the soma. To model the mIPSC, we randomly distributed 100 synaptic inputs along the apical dendrite and soma within this range of 200 µm from the soma. The current evoked by each input was recorded at the soma and averaged. A synaptic weight of 485 pS was required to generate an average mIPSC of amplitude of 12.8 pA recorded at the soma, similar to that recorded experimentally 12.7 with the same kinetics and amplitude (Fig. 2). This weight was used to replicate all the further IPSCs with the assumption that the weight for the $W_{py} = W_{SST} = 485 \text{ pS}.$

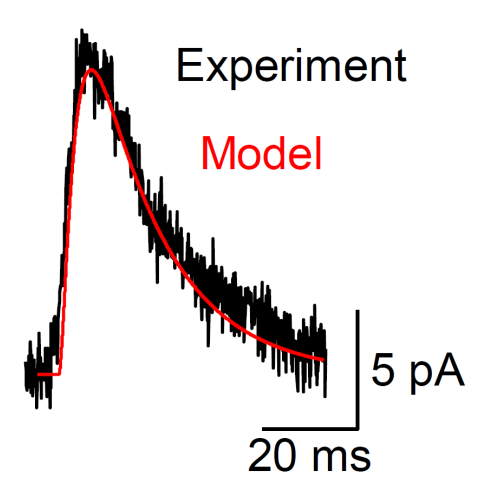


Figure 2: Comparison of somatic mIPSCs recorded experimentally and generated through the model. Comparison of somatic mIPSCs recorded experimentally (*black*) and generated through the model (*red*). The black trace represents the average of 20 mIPSCs recorded at a holding potential of 0 mV. A synaptic weight of 485 pS was set to replicate the oIPSC recorded experimentally in our model with similar kinetics..

Restricting the spatial distribution of the inhibitory inputs

CA1-PCs serve as the primary output neurons of the hippocampus. These cells receive synaptic excitation from distinct afferent pathways that target the proximal and distal domains of the dendritic arbor. Inhibitory input from local INs counteracts dendritic excitation. These neighboring INs differ widely in morphology, gene expression, physiology, and connectivity (Klausberger and Somogyi 2008). In our experiments, we focused on the inhibition of CA1-PCs by two types of GABAergic INs: (i) PV-INs and (ii) SST-INs. As stated previously, in CA1-PCs, proximal inhibition is largely provided by PV-INs, whereas distal inhibition is provided mostly but not exclusively by SST-INs.

PV-INs primarily target the proximal apical dendrites and soma of CA1-PCs, forming synapses within 50 μ m of the soma (Bloss et al. 2016). To reflect this distribution, we used NRN-EZ to place PV inhibitory synapses within a radial range of 25 \pm 25 μ m, ensuring an accurate spatial representation of perisomatic inhibition. These PV synapses were allocated across both the soma and the proximal apical dendrites.

SST-INs primarily target distal apical dendrites of CA1-PCs, forming synapses at distances >200 μ m from the soma (Bloss et al., 2016). Using NRN-EZ, we placed SST inhibitory synapses within a radial range of 0 ± 165 μ m from 'Apical' segment 319, which was 365 μ m away from the soma. In this way, we were able to distribute the SST-expressing GABAergic inputs over the apical dendrites starting from 200 μ m away from the soma.

Setting the release probability of inhibitory inputs

Neurotransmitter releases triggered by each action potential have a certain probability, which defines the synapse's reliability in transmitting the signal. This contributes to its overall average strength. (Del Castillo and Katz 1954). The probability that a synaptic vesicle will release its neurotransmitter content in response to an action potential is called release probability (P). Previous work has indicated that ppv=0.8 at $[Ca^{2+}]_o=2$ mM. Considering there is a 4th power relationship between release probability and $[Ca^{2+}]_o$, ppv=0.1 at $[Ca^{2+}]_o=1.2$ mM (**Fig. 3**, magenta).

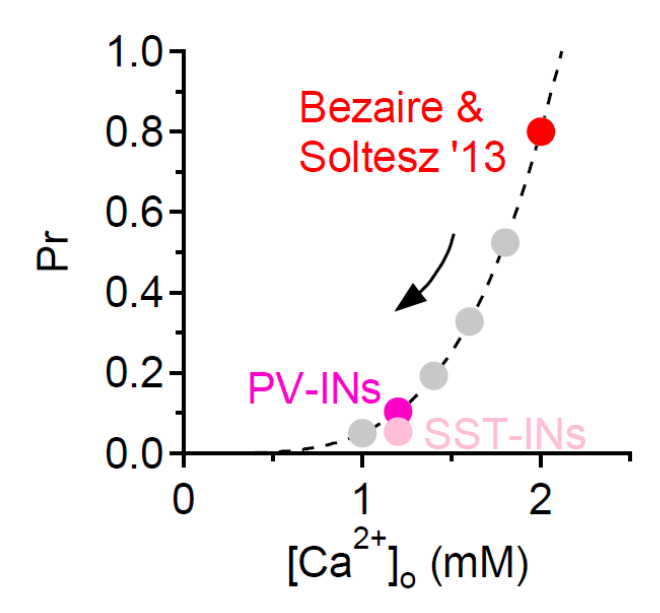


Figure 3: Power relationship describing the Ca²⁺-sensitivity of the release probability. The red dot represents the value of Pr of PV-to-CA1-PC inputs estimated in previous work with =2.0 mM. The relationship was used to estimate Pr for PV-to-CA1-PC inputs in our recording conditions, where =1.2 mM (magenta). Pr for SST-inputs was calculated by dividing the number of estimated SST inputs by the number of active inputs that were recruited to mimic the oIPSCs recorded experimentally (pink).

Effect of glutamate spillover on proximal and distal inhibition

During the patch clamp experiments (done by *Maurice Petroccione* from the lab), stereotaxic injections of a floxed viral construct encoding ChR2 were done in the CA1 region of both *Pvalb*^{Cre/+} and *Sst*^{Cre/+} mice (**Fig. 4a**). Optically evoked IPSCs (oIPSCs) were then recorded from CA1-PCs following the stimulation of either PV- or SST-INs. DHK reduced the amplitude of oIPSCs from PV-INs to 74±8% of baseline (n=10; *p=0.011; **Fig. 4b-e**). A similar reduction of oIPSCs from SST-INs was observed in response to DHK application (74±4% n=10; ***p=7.9e-5; **Fig. 4f-i**).

Previous studies on synaptic scaling have shown that a higher number of inputs at the distal end compensates for the dendritic attenuation (Andrasfalvy and Magee 2001; Bloss et al. 2016). Here, we wanted to see if glutamate spillover causes more effect on the distal dendrites by activating more mGLURIII receptors compared to those at the proximal end. We first distributed the PV and SST inhibitory inputs using NRN-EZ. The PV inputs were distributed within a distance of 50 µm, and SST inputs were distributed 200 µm away from the soma (Fig. 4j). To do this, we replicated the experimentally recorded oIPSC from PV-INs and iterated the simulation 100 times using different numbers of PV inputs for each simulation. Based on our optogenetics experiments, 4 active PV release sites were required to evoke an oIPSC (amp=67.22 pA, rise the olPSC time=4.12. t_{50} =20.54) comparable to evoked (amp=64.49 \pm 8.88, rise time=51.13 \pm 9.75, t_{50} =1.19). Therefore, we estimated a total of 4/0.1=40 PV release sites targeted CA1-PC in our model. EM reconstructions have

estimated that the number of SST inputs onto CA1-PCs is 8.3 times larger than that of PV-INs (Bloss et al. 2016), so the total number of SST inputs was estimated to be $40 \cdot 8.3 = 332$. For SST, it took 18 inputs to replicate the oIPSC (amp=56.90 pA, rise time= 6.00 ms, t_{50} = 36.89 ms) comparable to the one recorded experimentally (amp= 58.02 ± 11.73 pA, rise time= 5.78 ± 0.65 ms, t_{50} = 37.21 ± 6.68 ms), leading to pSST=18/332=0.05 (**Fig. 3**, pink).

DHK was used to block the major glutamate transporter GLT-1; this resulted in facilitating glutamate spillover and, in turn, activating the presynaptic mGLURIII receptors present on the GABAergic terminals. To replicate the DHK current recordings, we used the same approach as used for Control experiments. It was observed that a total of 3 inputs were required to produce the oIPSC (amp=51.88 pA, rise time= 4.17 ms, t_{50} = 21.17 ms,) which is comparable to the one recorded experimentally (amp= 51.13±9.75 pA, rise time=3.3±0.4, t_{50} =21.10±1.50) (**Fig. 4k**, *top*). Similarly, a total of 13 SST inputs reproduced the oIPSC (amp= 41.96 pA, rise time=5.45 ms, t_{50} = 37.24 ms), which is comparable to that with the experimental recordings (amp= 45.5 pA, rise time=5.46±0.72 ms, t_{50} = 37.38±77.15 ms) (**Fig. 4k**, *bottom*). Each simulation was repeated 100 times, each time randomizing the location of the active inputs. Therefore, the results represent the average of 100 simulations.

Different presynaptic factors could lead to a reduction of the IPSC amplitude: (i) the size of the readily releasable pool of GABA vesicles (RRP, comprised of N releases sites); (ii) release probability (P); (iii) quantal size (q).

In this model, we operationally define the number of release sites (N) as the number of presynaptic terminals (active zones) capable of releasing GABA. The readily releasable pool (RRP) refers to the collection of docked and primed vesicles that are immediately available for release at these sites. While multiple vesicles may exist at a single site, we assume that each release site contributes one vesicle to the RRP, consistent with models of low release probability synapses. Under this assumption, a reduction in the number of active release sites corresponds directly to a reduction in the RRP size. We acknowledge that this is a simplification and that synapses with multivesicular release may deviate from this model.

Experimental recordings from the lab (Petroccione et al., data not shown) tested whether the mGluRIII-mediated reduction in inhibitory transmission following DHK application was due to a change in the size of the readily releasable pool (RRP), release probability (P), or quantal size (q). mIPSCs recorded in the presence of TTX revealed no change in amplitude or kinetics following DHK application (amp: 97±4%, p=0.48; t50: 100±3%, p=0.87; rise: 98±6%, p=0.74), suggesting no change in q. Further, paired-pulse and train stimulation experiments showed that DHK reduced the RRP size (to 57±6% of baseline, ***p=1.0e-5), but not P (94±8%, p=0.45) or the replenishment rate (91±9%, p=0.33). These findings indicate that glutamate spillover reduces inhibition onto CA1-PCs primarily by reducing the number of RRP at GABAergic terminals, rather than by changing the probability or size of release events.

A 25-28% reduction in the amplitude of somatically-recorded PV- or SST-oIPSCs (**Fig. 4e,i**) can be obtained by reducing the total number of PV release sites from 40 to 30 and that of SST-INs from 332 to 260. This corresponds to a reduction in the number of active release sites of PV-INs from 4 to 3 and of SST-INs from 18 to 13 (a 25% and 28% reduction, respectively). The results from this simulation suggest that experimental conditions that promote glutamate spillover and mGluRIII activation do not change the relative strength of proximal vs distal inhibition onto CA1-PCs (**Fig. 4I**).

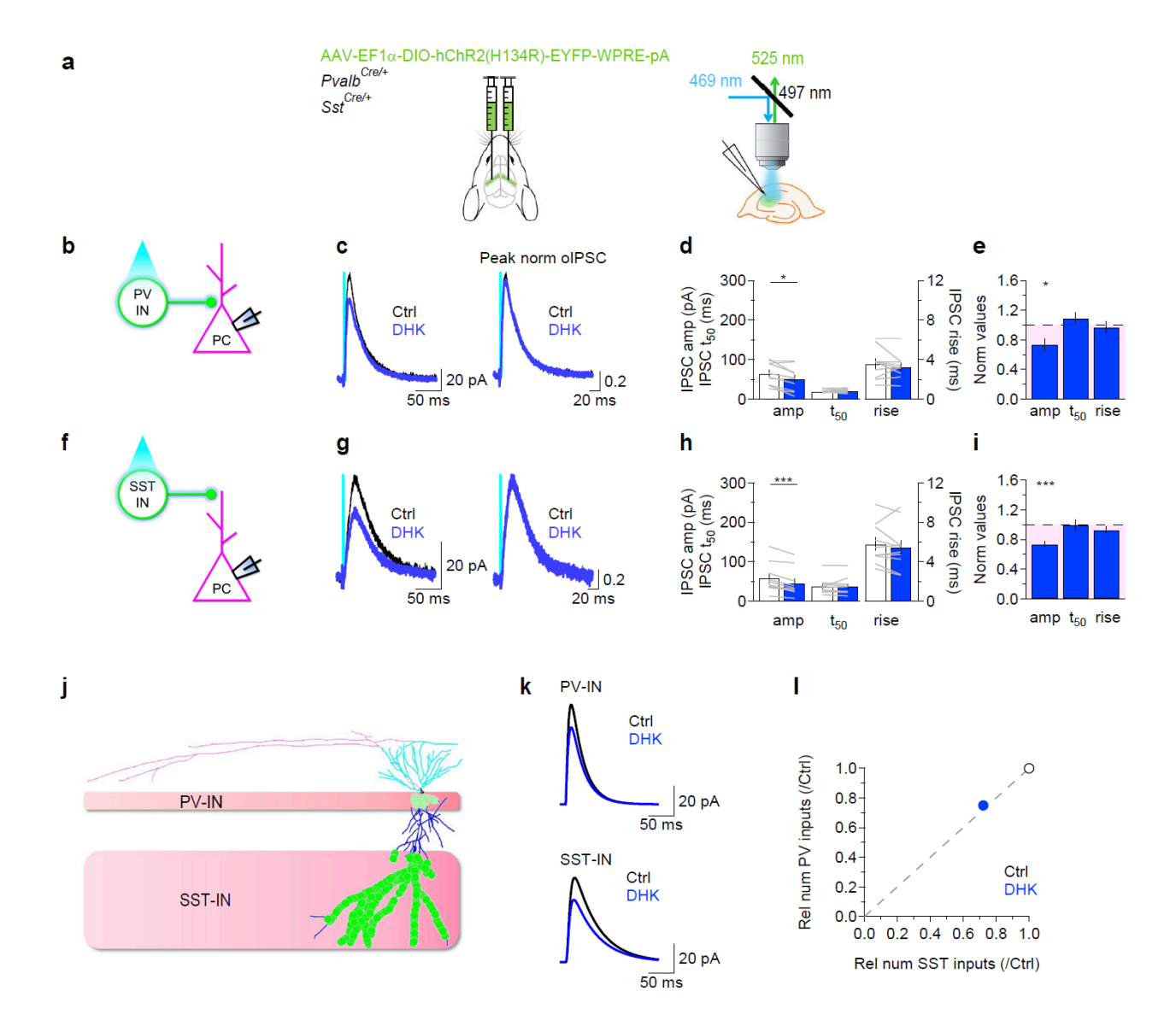


Figure 4. Proximal and distal inhibition onto CA1-PCs are modulated by mGluRIII. (a-i, data based on experiments conducted by other lab members, j-l data from computational model) (a) Schematic representation of the stereotaxic injections of viral constructs encoding ChR2 in hippocampal area CA3 of Pvalb^{Cre/+} and Sst^{Cre/+} mice and of the experiment settings. (b) Scheme describing optogenetic activation of PV-INs. (c) oIPSCs evoked by optical stimulation of PV-INs before (black) and after DHK (100 μM; blue). The traces on the right are normalized by the iIPSC peak. (d) Summary of the effect of DHK on the oIPSC amplitude and kinetics, in Pvalb^{Cre/+} mice. (e) Summary of the effect of DHK on the oIPSC

amplitude and kinetics, normalized by their values in control conditions. **(f-i)** As in B-E, for oIPSCs evoked by optical stimulation of SST-INs. **(j)** Morphology of a CA1-PCs receiving PV-inputs onto the soma and the proximal portion of the apical dendrite (0-50 μ m; *light green dots*), or SST-inputs onto the distal portion of the apical dendrite (>200 μ m; *green dots*). **(k)** Example of oIPSCs generated with a compartmental model of a CA1-PCs in response to activation of PV- (*top*) or SST-inputs (*bottom*). The model reproduces the effect of DHK on the amplitude and kinetics of these events detected experimentally (c, g). **(I)** A 25-28% reduction in the amplitude of the oIPSC recorded at the soma can be obtained by reducing the number of active PV-inputs from 4 to 3, and that of SST-inputs from 11 to 8. The scatter plot shows these results as relative effects in control conditions (*black*) and in DHK (*blue*).

The experimental data from the lab showed that the number of spines increased by 25% in the $A\beta_{42}$ mouse model and a 30% increase in the number of PV inputs. Though we see no change in the number of inputs from SST-INs, an increase in the number of spines and PV inputs is expected to alter the firing output of these CA1-PC. Given this simultaneous enhancement of both excitatory and inhibitory input convergence, we predicted that the net effect on the firing output of CA1-PCs would depend on the relative balance between these opposing forces. Our modeling efforts thus aimed to investigate which type of input—excitatory or inhibitory—has a predominant influence on neuronal output under these altered synaptic conditions.

Determining the synaptic weight of the excitatory synapses

Previous studies indicate that the linear density of spines along apical dendrites of CA1-PCs in the *stratum radiatum* of the mouse hippocampus is 2.8 μ m⁻¹ (Bloss et al. 2018). The total dendritic length in our CA1-PC model is 3,810.28 μ m. Therefore, the estimated total number of excitatory synaptic inputs onto our model cell is 2.8·3,810.28=10,669. The release probability for excitatory synapses at [Ca²⁺]_o = 2.5 mM is $P_{\rm exc}$ =0.3. Given that there is a fourth power relationship between [Ca²⁺]_o and $P_{\rm exc}$, we estimate $P_{\rm exc}$ to be 0.02 at [Ca²⁺]_o of 1.2 mM.

Each excitatory synapse expresses AMPA and NMDA receptors, and in our model we need to provide estimates of the synaptic weight for AMPA and NMDA receptors (W). This corresponds to the quantal size of mEPSCs, which can be estimated from patch-clamp recordings. Therefore, for AMPA receptors, the value of W at time 0 (i.e., W0) was calculated from experimentally recorded mEPSCs. This was done in the same way as the mIPSCs were modeled by distributing excitatory inputs within 200 µm from the soma. We used the following rationale. To generate mEPSCs with a mean amplitude of 14 pA, we need to set W0=0.43 nS. To reproduce the kinetics (rise and decay time) of experimentally recorded mEPSCs, we need to set the rise and decay time in the simulations to 0.2 ms and 2 ms, respectively. There is also evidence that the weight of AMPA-containing excitatory synapses varies along the length of dendrites. This phenomenon, commonly referred to as synaptic scaling, has been described in a series of dendritic patch-clamp recordings in the past. (Andrasfalvy and Magee 2001). Based on this data, we formulate the distance-dependent conductance of our AMPA receptors. This can be given with the equation as:

$$W = W0 + (1.7 * W0)/(1 + exp(-(d - 137)/38))$$

Here, *W* is the synaptic weight (i.e., the conductance) of AMPA receptors distributed on apical dendrites at a distance *d* from the soma.

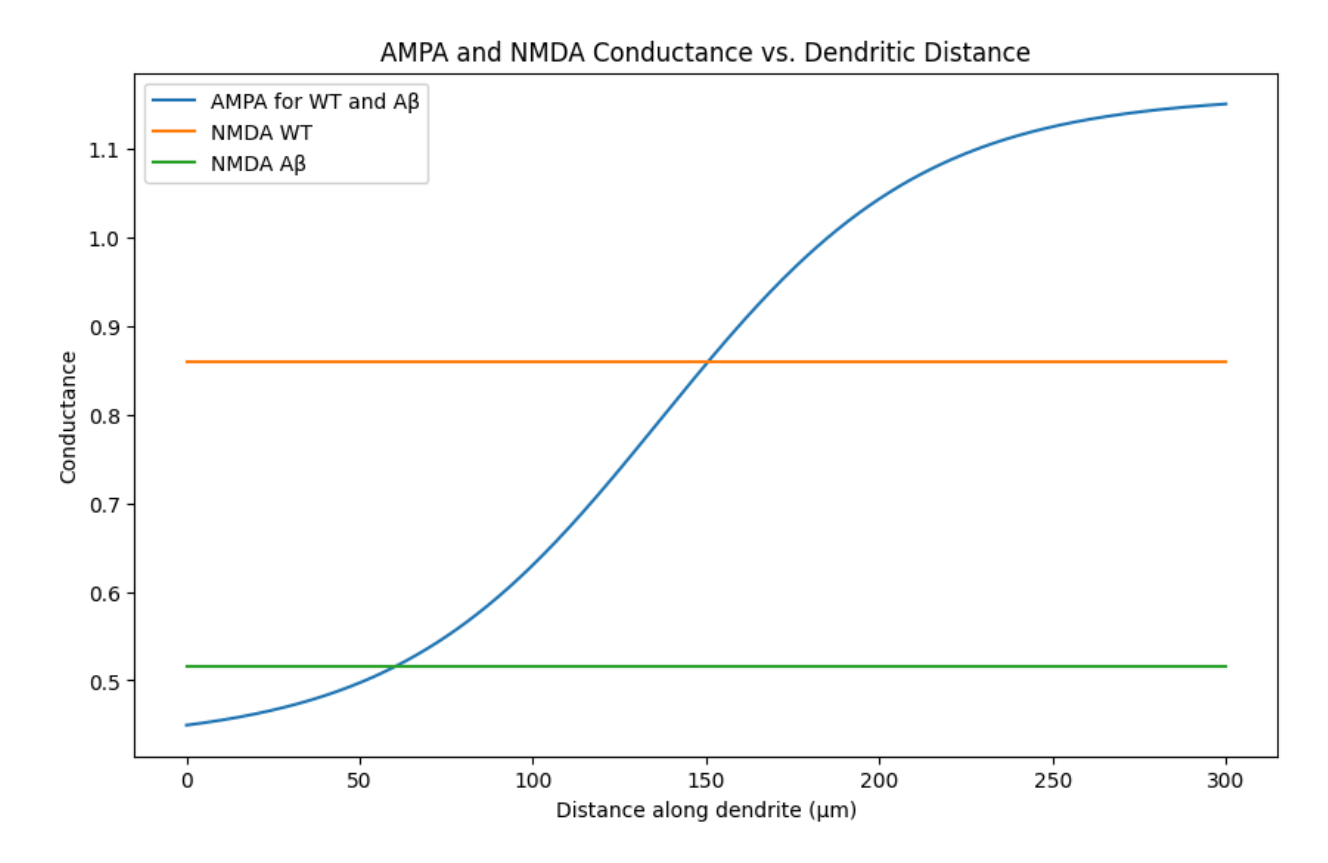


Figure 5. AMPA and NMDA conductance as a function of distance from the soma in our model. AMPA conductance (*blue*) increases with distance, following a sigmoidal profile. NMDA conductance is held constant across all distances. Experimentally measured NMDA/AMPA ratios are higher in WT (orange, ratio = 2.0) compared to $A\beta_{42}$ neurons (green, ratio = 1.2), reflecting a relative reduction in NMDA receptor contribution in the $A\beta_{42}$ condition.

Our lab experiments showed that the NMDA/AMPA ratio in CA1-PCs of wild type (WT) and A β_{42} -AAV mice is ~2 and ~1.2, respectively. Given that there is no known synaptic scaling rule for NMDA receptors, this value was kept at the same value along the entire apical dendritic arbor. In our simulations, we set the synaptic weight of NMDA receptors to 8.6e-4 S/cm² for WT mice and 5.2e-4 S/cm² for A β_{42} -AAV mice, respectively.

Effect of $A\beta_{42}$ on integration of excitatory and inhibitory inputs

Following the incorporation of ion channel mechanisms and other biophysical parameters (as detailed in the *Methods* section), excitatory synapses comprising both AMPA and NMDA receptor components were distributed across the dendritic arbor. The total number of excitatory synapses in the WT model was estimated to be 10,669,

whereas the $A\beta_{42}$ model exhibited an increased count of 13,870 synapses, consistent with the observed increase in spine density. Since the estimated release probability for our excitatory inputs is (P_{exc}) 0.02, this yielded 213 active excitatory inputs in the WT model and 277 active excitatory inputs in the $A\beta_{42}$ model. Similarly, the number of active PV inputs was increased from 6 to 9, whereas the number of active SST inputs remained constant at 25. The synaptic weight and release probability were determined from the voltage-clamp mIPSC experiments. The synaptic weight for the inhibitory inputs was set to be 6.6e-3 to replicate the mIPSCs recorded experimentally.

The inputs were fired at a collective frequency of 0-50 Hertz in a gaussian manner with a standard deviation of 10 Hz. The aim was to do this till 100 Hz but due to time constraints and computational limitation we were only able to map the firing output of the cell from 0-50 Hz. After iterating the simulations 10 times, we generated an average heatmap that showed the firing output of CA1-PCs in WT and $A\beta_{42}$ mice recorded at the soma. The mean number of action potentials recorded at the soma in response to 50 Hz stimulation was 7.3 in the $A\beta_{42}$ model and 7.3 in the WT model.

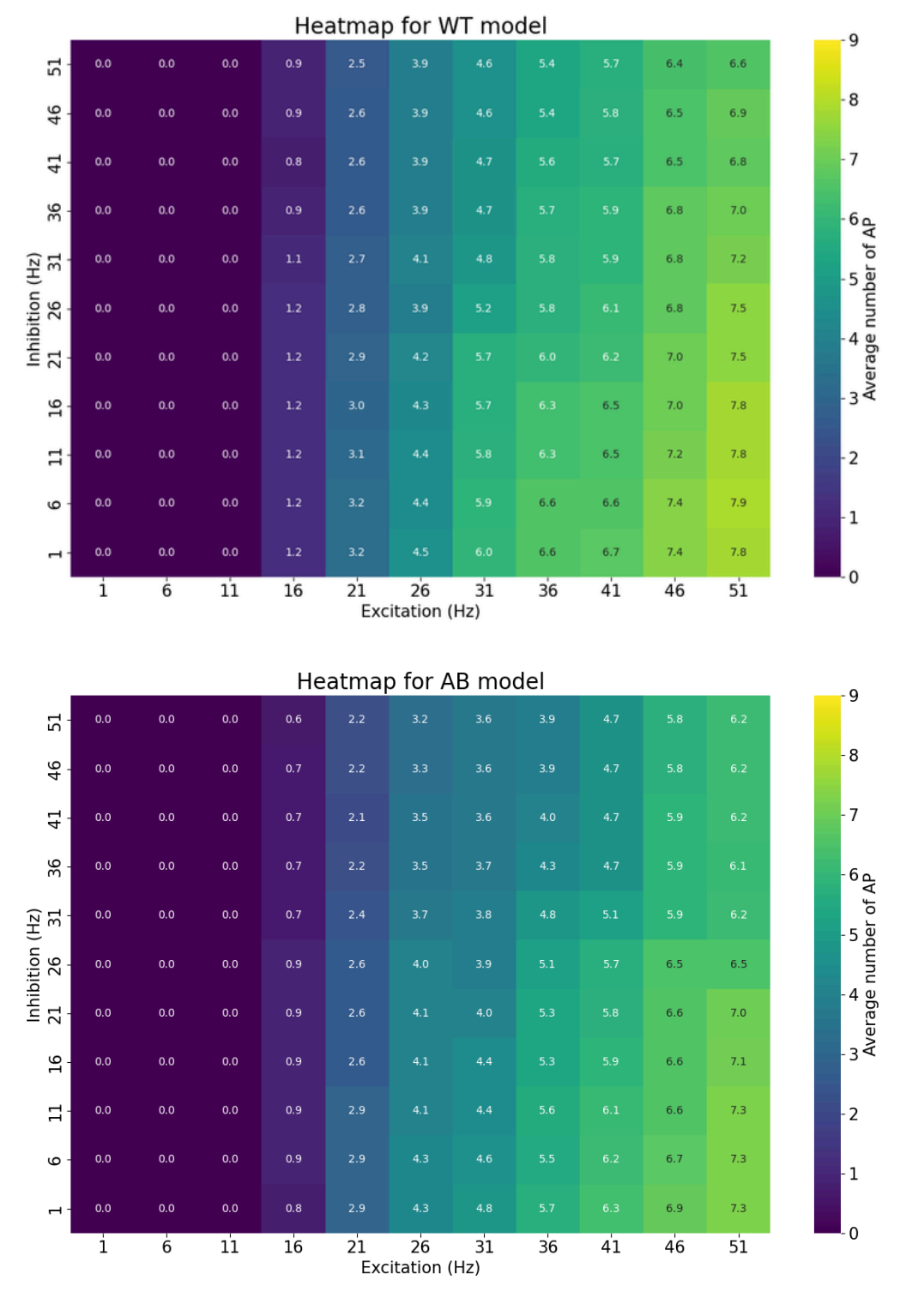


Figure 6. Firing output of CA1-PC in WT and $A\beta_{42}$ mice. Heatmap showing the number of action potential generated by CA1-PCs using different frequencies for excitatory and inhibitory inputs

Chapter 4 - Discussion

Our results show that spillover activation of mGluRIII reduces PV- and SST-inhibition onto CA1-PCs to a similar extent. How come the effects of spillover are similar for proximal and distal synapses? One factor that could contribute to this result is the fact that the nearest neighbor distance between excitatory and inhibitory synapses formed by PV- and SST-INs onto CA1-PCs is fairly similar (Herde et al. 2020; Scanziani et al. 1997; Ventura and Harris 1999). This means that they are equally susceptible to the effect of glutamate transporter blockade.

Proximal and distal inhibition control different aspects of synaptic integration in CA1-PCs. PV-INs are potent inhibitors of action potential generation at the axon initial segment. By contrast, SST-INs limit synaptic integration of distal excitatory inputs, which reach CA1-PCs through axonal projections from extra-hippocampal regions like the entorhinal cortex (Pelkey et al. 2017). The fact that glutamate spillover can tune the strength of these two different types of spatially segregated inputs suggests that the regulation of inter-synaptic independence is a critical mechanism that can regulate the computational skills of CA1-PCs. Since these cells provide spatial representations of the external environment, these findings indicate that spillover powerfully controls the accuracy of our representation of the external world.

While our model reproduces this reduction in oIPSC amplitude by decreasing the number of active release sites (from $4\rightarrow 3$ for PV and $18\rightarrow 13$ for SST inputs), we recognize that alternate parameter combinations—such as partial reductions in P or q—could theoretically yield similar somatic currents. However, given that the experimental kinetics remain unchanged and paired-pulse ratios are unaffected, our modeling decision to selectively reduce N is the most constrained and biophysically plausible explanation.

We did not explicitly test whether mGluRIII activation via glutamate spillover changes in $A\beta_{42}$ mice. In fact, this is something that we would like to pursue with future investigations. Our analysis of $A\beta_{42}$ mice showed that there are: (i) more inhibitory synapses (likely from PV-INs); (ii) more excitatory synapses; (iii) at each excitatory synapse, fewer NMDA receptors are activated. We then used a modeling approach to determine whether they lead to increased or reduced action potential firing in CA1-PCs. Our findings indicate that the combined effect of more PV inputs and reduced NMDA conductance results in a lesser number of action potentials and in turn, lesser firing of the cell. More PV inputs increase the probability of an input lying closer to the soma and inhibiting the generation of an action potential that is recorded at the soma. activation is reduced.

The results shown in the heatmap represent simulations where only 0-50 excitatory synaptic inputs were randomly selected and activated from a larger pool of 213 excitatory inputs, rather than simulating all 213 inputs firing 0-50 times each (i.e., at

0-50 Hz). Though the results shown in the Fig. 6 do not show a significant change in the two cases, this approach was useful to explore the relative influence of synaptic changes and to evaluate the current implementation of the model without introducing excessive network activity or unrealistic firing patterns. Our future plans include larger scale investigations where all 213 inputs are active at a broader range of frequencies (0-100 Hz). This range of activity is consistent with that occurring in the hippocampus during learning and memory, commonly known as the gamma range (Buzsáki and Moser 2013; Chrobak, Lörincz, and Buzsáki 2000).

Due to computational constraints and time limitations, we were unable to fully test the model by running extended simulations in which the entire synaptic population would fire at a combined frequency of 100 Hz. Nonetheless, the results we obtained — even with only a subset of synapses activated — consistently demonstrated a reduction in somatic firing in the $A\beta_{42}$ condition. This suggests that the inhibitory influence of increased PV input, combined with reduced NMDA receptor activation, exerts a strong suppressive effect on CA-PC excitability.

We anticipate that future simulations involving higher input frequencies and activation of the full synaptic population will help confirm and extend these findings. Such work will allow us to test whether the observed trends are amplified under more realistic network activity and further refine our understanding of excitability alterations in $A\beta_{42}$ pathology.

References

- Buzsáki G, Moser El. Memory, navigation and theta rhythm in the hippocampal-entorhinal system. Nat Neurosci. 130-8.
- Chrobak JJ, Lörincz A, Buzsáki G. Physiological patterns in the hippocampo-entorhinal cortex system. Hippocampus. 2000;10(4):457-65. Bibliography
- Alzheimer's Association (2014), "2014 Alzheimer's disease facts and figures.," Alzheimer's & Dementia, 10 (2), e47-92.
- Andrasfalvy, B K and J C Magee (2001), "Distance-dependent increase in AMPA receptor number in the dendrites of adult hippocampal CA1 pyramidal neurons.," *The Journal of Neuroscience*, 21 (23), 9151–59.
- Baskys, A and R C Malenka (1991), "Agonists at metabotropic glutamate receptors presynaptically inhibit EPSCs in neonatal rat hippocampus.," *The Journal of Physiology*, 444, 687–701.
- Bettler, B, K Kaupmann, and N Bowery (1998), "GABAB receptors: drugs meet clones.," *Current Opinion in Neurobiology*, 8 (3), 345–50.
- Bettler, Bernhard, Klemens Kaupmann, Johannes Mosbacher, and Martin Gassmann (2004), "Molecular structure and physiological functions of GABA(B) receptors.," *Physiological Reviews*, 84 (3), 835–67.
- Bloss, Erik B, Mark S Cembrowski, Bill Karsh, Jennifer Colonell, Richard D Fetter, and Nelson Spruston (2016), "Structured Dendritic Inhibition Supports Branch-Selective Integration in CA1 Pyramidal Cells.," *Neuron*, 89 (5), 1016–30.
- Bloss, Erik B, Mark S Cembrowski, Bill Karsh, Jennifer Colonell, Richard D Fetter, and Nelson Spruston (2018), "Single excitatory axons form clustered synapses onto CA1 pyramidal cell dendrites.," *Nature Neuroscience*, 21 (3), 353–63.
- Bormann, J (2000), "The 'ABC' of GABA receptors.," *Trends in Pharmacological Sciences*, 21 (1), 16–19.
- Brickley, Stephen G and Istvan Mody (2012), "Extrasynaptic GABA(A) receptors: their function in the CNS and implications for disease.," *Neuron*, 73 (1), 23–34.
- Buzsáki, György and Edvard I Moser (2013), "Memory, navigation and theta rhythm in the hippocampal-entorhinal system.," *Nature Neuroscience*, 16 (2), 130–38.
- Chiu, Delia N and Craig E Jahr (2017), "Extracellular Glutamate in the Nucleus Accumbens Is Nanomolar in Both Synaptic and Non-synaptic Compartments.," *Cell reports*, 18 (11), 2576–83.
- Chrobak, J J, A Lörincz, and G Buzsáki (2000), "Physiological patterns in the hippocampo-entorhinal cortex system.," *Hippocampus*, 10 (4), 457–65.
- Clements, J D, R A Lester, G Tong, C E Jahr, and G L Westbrook (1992), "The time course of glutamate in the synaptic cleft.," *Science*, 258 (5087), 1498–1501.
- Cobb, Evan A W, Maurice A Petroccione, and Annalisa Scimemi (2023), "NRN-EZ: an

- application to streamline biophysical modeling of synaptic integration using NEURON.," *Scientific Reports*, 13 (1), 464.
- Danbolt, N C (2001), "Glutamate uptake.," Progress in Neurobiology, 65 (1), 1–105.
- Del Castillo, J and B Katz (1954), "Quantal components of the end-plate potential.," *The Journal of Physiology*, 124 (3), 560–73.
- Desai, M A, C J McBain, J A Kauer, and P J Conn (1994), "Metabotropic glutamate receptor-induced disinhibition is mediated by reduced transmission at excitatory synapses onto interneurons and inhibitory synapses onto pyramidal cells.," *Neuroscience Letters*, 181 (1–2), 78–82.
- Enz, R and G R Cutting (1999), "GABAC receptor rho subunits are heterogeneously expressed in the human CNS and form homo- and heterooligomers with distinct physical properties.," *The European Journal of Neuroscience*, 11 (1), 41–50.
- Farrant, Mark and Zoltan Nusser (2005), "Variations on an inhibitory theme: phasic and tonic activation of GABA(A) receptors.," *Nature Reviews. Neuroscience*, 6 (3), 215–29.
- Fonnum, F (1984), "Glutamate: a neurotransmitter in mammalian brain.," *Journal of Neurochemistry*, 42 (1), 1–11.
- Gabitto, Mariano I, Kyle J Travaglini, Victoria M Rachleff, Eitan S Kaplan, Brian Long, Jeanelle Ariza, Yi Ding, Joseph T Mahoney, Nick Dee, Jeff Goldy, Erica J Melief, Anamika Agrawal, Omar Kana, Xingjian Zhen, Samuel T Barlow, Krissy Brouner, Jazmin Campos, John Campos, Ambrose J Carr, Tamara Casper, and Ed S Lein (2024), "Integrated multimodal cell atlas of Alzheimer's disease.," *Nature Neuroscience*, 27 (12), 2366–83.
- Gereau, R W and P J Conn (1995), "Multiple presynaptic metabotropic glutamate receptors modulate excitatory and inhibitory synaptic transmission in hippocampal area CA1.," *The Journal of Neuroscience*, 15 (10), 6879–89.
- Häusser, M and A Roth (1997), "Estimating the time course of the excitatory synaptic conductance in neocortical pyramidal cells using a novel voltage jump method.," *The Journal of Neuroscience*, 17 (20), 7606–25.
- Herde, Michel K, Kirsten Bohmbach, Cátia Domingos, Natascha Vana, Joanna A Komorowska-Müller, Stefan Passlick, Inna Schwarz, Colin J Jackson, Dirk Dietrich, Martin K Schwarz, and Christian Henneberger (2020), "Local Efficacy of Glutamate Uptake Decreases with Synapse Size.," *Cell reports*, 32 (12), 108182.
- Herman, Melissa A and Craig E Jahr (2007), "Extracellular glutamate concentration in hippocampal slice.," *The Journal of Neuroscience*, 27 (36), 9736–41.
- Hille, B (1992), "G protein-coupled mechanisms and nervous signaling.," *Neuron*, 9 (2), 187–95.
- Hines, M L and N T Carnevale (1997), "The NEURON simulation environment.," *Neural Computation*, 9 (6), 1179–1209.
- Klausberger, Thomas and Peter Somogyi (2008), "Neuronal diversity and temporal

- dynamics: the unity of hippocampal circuit operations.," Science, 321 (5885), 53-57.
- Lehre, K P and N C Danbolt (1998), "The number of glutamate transporter subtype molecules at glutamatergic synapses: chemical and stereological quantification in young adult rat brain.," *The Journal of Neuroscience*, 18 (21), 8751–57.
- Li, Songting, Nan Liu, Li Yao, Xiaohui Zhang, Douglas Zhou, and David Cai (2019), "Determination of effective synaptic conductances using somatic voltage clamp.," *PLoS Computational Biology*, 15 (3), e1006871.
- Masu, M, Y Tanabe, K Tsuchida, R Shigemoto, and S Nakanishi (1991), "Sequence and expression of a metabotropic glutamate receptor.," *Nature*, 349 (6312), 760–65.
- Mayer, M L, G L Westbrook, and L Vyklický (1988), "Sites of antagonist action on N-methyl-D-aspartic acid receptors studied using fluctuation analysis and a rapid perfusion technique.," *Journal of Neurophysiology*, 60 (2), 645–63.
- McCauley, John P, Maurice A Petroccione, Lianna Y D'Brant, Gabrielle C Todd, Nurat Affinnih, Justin J Wisnoski, Shergil Zahid, Swasti Shree, Alioscka A Sousa, Rose M De Guzman, Rosanna Migliore, Alexey Brazhe, Richard D Leapman, Alexander Khmaladze, Alexey Semyanov, Damian G Zuloaga, Michele Migliore, and Annalisa Scimemi (2020), "Circadian modulation of neurons and astrocytes controls synaptic plasticity in hippocampal area CA1.," *Cell reports*, 33 (2), 108255.
- Migliore, Rosanna, Carmen A Lupascu, Luca L Bologna, Armando Romani, Jean-Denis Courcol, Stefano Antonel, Werner A H Van Geit, Alex M Thomson, Audrey Mercer, Sigrun Lange, Joanne Falck, Christian A Rössert, Ying Shi, Olivier Hagens, Maurizio Pezzoli, Tamas F Freund, Szabolcs Kali, Eilif B Muller, Felix Schürmann, Henry Markram, and Michele Migliore (2018), "The physiological variability of channel density in hippocampal CA1 pyramidal cells and interneurons explored using a unified data-driven modeling workflow.," *PLoS Computational Biology*, 14 (9), e1006423.
- Morishita, W, S A Kirov, and B E Alger (1998), "Evidence for metabotropic glutamate receptor activation in the induction of depolarization-induced suppression of inhibition in hippocampal CA1.," *The Journal of Neuroscience*, 18 (13), 4870–82.
- Nowak, L, P Bregestovski, P Ascher, A Herbet, and A Prochiantz (1984), "Magnesium gates glutamate-activated channels in mouse central neurones.," *Nature*, 307 (5950), 462–65.
- Nusser, Z, W Sieghart, D Benke, J M Fritschy, and P Somogyi (1996), "Differential synaptic localization of two major gamma-aminobutyric acid type A receptor alpha subunits on hippocampal pyramidal cells.," *Proceedings of the National Academy of Sciences of the United States of America*, 93 (21), 11939–44.
- Pelkey, Kenneth A, Ramesh Chittajallu, Michael T Craig, Ludovic Tricoire, Jason C Wester, and Chris J McBain (2017), "Hippocampal gabaergic inhibitory interneurons.," *Physiological Reviews*, 97 (4), 1619–1747.
- Poncer, J C, H Shinozaki, and R Miles (1995), "Dual modulation of synaptic inhibition by

- distinct metabotropic glutamate receptors in the rat hippocampus.," *The Journal of Physiology*, 485 (Pt 1) (Pt 1), 121–34.
- Salt, T E and S A Eaton (1995), "Modulation of sensory neurone excitatory and inhibitory responses in the ventrobasal thalamus by activation of metabotropic excitatory amino acid receptors.," *Neuropharmacology*, 34 (8), 1043–51.
- Scanziani, M, B H Gähwiler, and S Charpak (1998), "Target cell-specific modulation of transmitter release at terminals from a single axon.," *Proceedings of the National Academy of Sciences of the United States of America*, 95 (20), 12004–9.
- Scanziani, M, P A Salin, K E Vogt, R C Malenka, and R A Nicoll (1997), "Use-dependent increases in glutamate concentration activate presynaptic metabotropic glutamate receptors.," *Nature*, 385 (6617), 630–34.
- Semyanov, A and D M Kullmann (2000), "Modulation of GABAergic signaling among interneurons by metabotropic glutamate receptors.," *Neuron*, 25 (3), 663–72.
- Shigemoto, R, A Kulik, J D Roberts, H Ohishi, Z Nusser, T Kaneko, and P Somogyi (1996), "Target-cell-specific concentration of a metabotropic glutamate receptor in the presynaptic active zone.," *Nature*, 381 (6582), 523–25.
- Sommer, B, M Köhler, R Sprengel, and P H Seeburg (1991), "RNA editing in brain controls a determinant of ion flow in glutamate-gated channels.," *Cell*, 67 (1), 11–19.
- Somogyi, Peter, Yannis Dalezios, Rafael Luján, J David B Roberts, Masahiko Watanabe, and Ryuichi Shigemoto (2003), "High level of mGluR7 in the presynaptic active zones of select populations of GABAergic terminals innervating interneurons in the rat hippocampus.," *The European Journal of Neuroscience*, 17 (12), 2503–20.
- Sperling, Reisa, Elizabeth Mormino, and Keith Johnson (2014), "The evolution of preclinical Alzheimer's disease: implications for prevention trials.," *Neuron*, 84 (3), 608–22.
- Ventura, R and K M Harris (1999), "Three-dimensional relationships between hippocampal synapses and astrocytes.," *The Journal of Neuroscience*, 19 (16), 6897–6906.
- Vogt, K E and R A Nicoll (1999), "Glutamate and gamma-aminobutyric acid mediate a heterosynaptic depression at mossy fiber synapses in the hippocampus.," *Proceedings of the National Academy of Sciences of the United States of America*, 96 (3), 1118–22.
- Williams, Stephen R and Simon J Mitchell (2008), "Direct measurement of somatic voltage clamp errors in central neurons.," *Nature Neuroscience*, 11 (7), 790–98.